ADVANCED HEALTHCARE MATERIALS
www.advhealthmat.de

Fillable Magnetic Microrobots for Drug Delivery to Cardiac Tissues In Vitro

*Maggie S. Chen, Rujie Sun, Richard Wang, Yuyang Zuo, Kun Zhou, Junyoung Kim, and Molly M. Stevens**

Many cardiac diseases, such as arrhythmia or cardiogenic shock, cause irregular beating patterns that must be regulated to prevent disease progression toward heart failure. Treatments can include invasive surgery or high systemic drug dosages, which lack precision, localization, and control. Drug delivery systems (DDSs) that can deliver cargo to the cardiac injury site could address these unmet clinical challenges. Here, a microrobotic DDS that can be mobilized to specific sites via magnetic control is presented. This DDS incorporates an internal chamber that can protect drug cargo. Furthermore, the DDS contains a tunable thermosensitive sealing layer that gradually degrades upon exposure to body temperature, enabling prolonged drug release. Once loaded with the small molecule drug norepinephrine, this microrobotic DDS modulated beating frequency in induced pluripotent stem-cell derived cardiomyocytes (iPSC-CMs) in a dose-dependent manner, thus simulating drug delivery to cardiac cells in vitro. The DDS also navigates several maze-like structures seeded with cardiomyocytes to demonstrate precise locomotion under a rotating low-intensity magnetic field and on-site drug delivery. This work demonstrates the utility of a magnetically actuating DDS for precise, localized, and controlled drug delivery which is of interest for a myriad of future opportunities such as in treating cardiac diseases.

1. Introduction

Cardiac diseases, a leading cause of death worldwide, are often treated through the administration of small molecule drugs such as metformin, norepinephrine, and amiodarone.[1] These drugs are routinely administered at high systemic dosages, which are often required to overcome the effects of circulation and diffusion[1,2] but can also lead to off-target effects, including negative impacts on the metabolism and survival of surrounding tissues.[2] These challenges motivate a significant clinical need for enhanced drug delivery systems (DDSs) that can traffic drug molecules or other therapeutic cargo directly to the injury site for controlled and localized drug release.[3] Currently, there are several DDSs in development for cardiac applications, including lipid-based nanoparticles,[4] hydrogels,[5] extracellular vesicles,[6] and polymeric nanoparticles.[7] Through selection of materials, these DDSs can be engineered to respond to external triggers such as heat[8] or pH.[9] Similarly, the materials comprising the system can be chosen to controllably degrade over time, providing a prolonged cargo release profile.[10] The surface of DDSs can be further functionalized using proteins or factors, such as myosin antibody fragments,[11] to promote greater localization of the carrier to the area of interest.[12] Other DDSs include Janus particles,[13] which can have two distinct domains with anisotropic compositions enabling different functions, as well as self-assembled peptide structures of which aggregation can be optimized via various outside factors (pH, temperature, etc).[14]

Despite the progress made in DDS development, nanocarrier-based DDSs in clinical trials for cardiac disease[15] have limited drug delivery efficiency. In particular, such systems have been reported to divert from the cardiovascular circulatory system into areas such as the respiratory and digestive tract or to negatively interact with the immune system, which leads to concerns regarding toxicity and localization.[16] While these systems can be functionalized with surface proteins or immunoglobulins to help traffic the carrier to the heart, they would still clearly depend on systemic circulation.[16] Cardiac delivery systems with more precise spatial movement and drug release profiles have the potential to improve localization without relying on systemic circulation. Toward this goal, magnetic actuation has been explored as a

M. S. Chen, R. Sun, R. Wang, Y. Zuo, K. Zhou, J. Kim, M. M. Stevens
Department of Materials
Department of Bioengineering
Institute of Biomedical Engineering
Imperial College London
London SW7 2AZ, UK
E-mail: molly.stevens@dpag.ox.ac.uk
M. M. Stevens
Kavli Institute for Nanoscience Discovery
Department of Physiology, Anatomy, & Genetics
Department of Engineering Science
University of Oxford
Oxford OX1 3QU, UK

The ORCID identification number(s) for the author(s) of this article can be found under https://doi.org/10.1002/adhm.202400419

DOI: 10.1002/adhm.202400419

control modality for improving localization and achieving higher degrees of spatial control while also maintaining the advantages of a biologically compatible, tunable DDS.[17] By leveraging magnetism as a non-invasive propulsion method, the DDSs become non-reliant on diffusion gradients and fluid circulation to guide movement.[18]

Furthermore, advances in catheterization technologies can be coupled with magnetic actuation to provide a further buffer against blood flow and to enable more localized procedural capabilities in the heart vasculature.[19] Catheter-based delivery approaches can allow for direct drug injection into cardiac areas, after which the drug can diffuse throughout the cardiac tissue.[20] Such catheters can be designed using soft materials,[21] can be magnetically actuated using an external magnetic field coupled with an articulating tip,[22] and can protect against external turbulent flow using incorporated stabilization mechanisms.[23] While these technologies offer promise to deliver drugs (or conduct cardiac procedures) in a localized and steerable fashion, there is a lack of control over the temporal dynamics of cargo delivery. The risk of vessel wall damage and lack of maneuverability in smaller vessels are also challenges.[20]

Previously, we developed a bio-inspired DDS based on the unique properties of puffball fungi: this system allows high-cargo loads to be protected from external environmental factors.[24] We further functionalized the DDS with a NIR-responsive polycaprolactone sealing layer to enable on-demand cargo release. However, due to the wide melting range and high melting point of the material, the system depends on NIR availability and light penetration and does not readily melt at body temperature (37 °C). Therefore, development of tunable thermosensitive dip-sealing materials could enable robust cargo release upon exposure to 37 °C and thus potentially address a gap in cardiac drug delivery applications. We envision potentially coupling this micororobot with catheter assistance for trafficking of the system into the vasculature of the heart, after which external magnetic actuation can be used to maneuver the microrobot through the smaller vessels in the heart for controlled drug delivery.

In this work, we present a fillable magnetic microrobot with tunable drug release capabilities based on a highly biocompatible, phase-change fatty acid sealing layer. We describe the microrobot fabrication technique and characterize the fatty acid mixtures used to achieve thermosensitivity and control over drug release mechanics. We then demonstrate the biocompatibility of the platform using induced pluripotent stem cell-derived cardiomyocytes (iPSC-CMs) as a model system for cardiac tissue. We characterize the functionality of the microrobots by modulating cardiomyocyte beating using a model drug. We further demonstrate magnetically-actuated locomotion of the microrobots to a target area followed by thermally-triggered drug release and subsequent change in the beating frequency of cardiomyocytes. This promising DDS overcomes previous challenges of drug delivery precision and control of spatial positioning and may be of interest for drug delivery to tissues beyond the heart.

2. Results and Discussion

2.1. Design and Fabrication of Microrobots

Several key factors informed the development of microrobots for cardiac drug delivery. First, we aimed to design a microrobot containing superficial pores for payload release and a fillable internal chamber for small molecule loading without necessitating chemical modification (**Figure 1**). We also sought to enable prolonged and controlled drug release into the outer environment with a thermosensitive sealing layer that would initially cover the superficial pores and degrade upon exposure to higher temperature. Finally, we aimed to incorporate magnetic properties into the microrobot in order to facilitate actuation under external magnetic fields and thereby provide fine-tuned movement and navigation. Microrobots with these collective properties would address several key limitations in existing DDSs for cardiac drug delivery applications, such as lack of spatial control and control over drug release mechanics. In a clinical setting, this design would allow the microrobot to be injected into the systemic circulation and then propelled via a controllable magnetic field to the area of interest, where the sealing layer would melt and thus gradually release the internal cargo (Figure 1).

The microrobot system was fabricated in four steps: i) two-photon polymerization (2PP)-based 3D microprinting to generate the microrobot body, ii) sputter coating with nickel (Ni) and titanium (Ti) to generate a magnetic outer layer, iii) drug loading through vacuum pressure, and iv) dip sealing with a thermosensitive fatty acid mixture (**Figure 2A**). Specifically, 2PP-based 3D microprinting was used to generate a spherical robot body 550 microns in diameter, with an array of seven pores on the top of the robot each with a diameter of 60 microns. Previously, several designs that varied the pore diameter or shape were tested, with the current design being selected as suitable for adequate drug release and loading.[24] While the aorta can be as large as 3 centimeters in diameter, other major blood vessels that provide input into the ventricles (such as the right and left coronary arteries) range from 2.5 to 3 centimeters in diameter.[25] Therefore, the 550 micron diameter of the microrobot enables mobility even within the narrower vessels near the heart. The 2PP technique is capable of high resolution printing of the small structural features seen on the microrobot and allows easy design modification during optimization and validation.[26] Furthermore, this technique enables simultaneous fabrication of microrobot arrays with high uniformity across all structures, and thus could be suitable for batch manufacturing in future scale-up. Next, vapor deposition was used to add thin layers of Ni and Ti, conferring magnetic properties and biocompatibility, respectively, onto the microrobots whilst enabling controlled locomotion of the microrobots via the low-intensity magnetic field. While Ni has demonstrated some degree of cytotoxicity when internalized into cells,[27] this technique utilizes an extremely thin layer of Ni. Furthermore, integration of a Ti sputter-coated layer can reduce risk of toxicity given that Ti is known for its high biocompatibility;[28] previously, NiTi alloys were demonstrated to be compatible with several cell types.[29] As a proof-of-concept for cargo loading, Rhodamine B (RhB; 1% w/v RhB in DMSO) was placed on top of the microrobots and transferred into the internal space by vacuum pressure. The use of DMSO as a solvent for poorly soluble drugs could be applied for drugs with a range of chemical properties, which broadens the potential drug delivery applications of our platform.[24,30] Each microrobot held 30.79 ± 5.73 nanoliters (nL) of solution (Figure 2B). Furthermore, 2 microrobots were calculated to hold 68.42 ± 7.24 nL of solution, highlighting the reliability and uniformity of the fabrication and loading process. Using optical microscopy, the pristine microrobot was colorless while

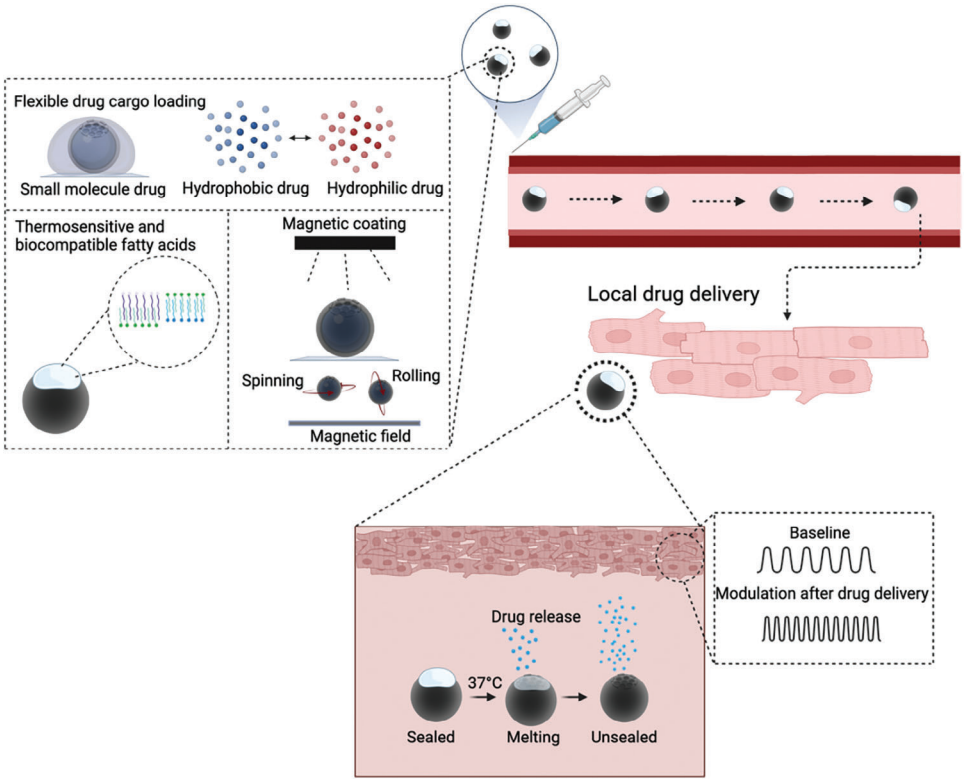

Figure 1. Tunable small molecule drug release from magnetically controlled microrobots sealed with thermosensitive and biocompatible fatty acid mixture can modify the pacing of cardiomyocytes.

the loaded microrobot displayed a pink solution encapsulated within the internal chamber, which served as visible evidence of successful loading (Figure 2A). Successful deposition of the magnetized outer layers was confirmed through energy-dispersive X-ray spectroscopy, which showed homogenous deposition of Ni and Ti on the microrobot surface (Figure 2C). Finally, the loaded microrobots were sealed using a mixture of fatty acids with a tunable eutectic melting point. Fatty acids are a critical component of natural fats found in the human body and in foods and thus highly biocompatible.[31] Conveniently, fatty acids are also known to be phase-change materials.[32] Using previously developed methods,[24] liquid fatty acids (such as lauric acid and stearic acid) were first spin-coated into a thin film before unsealed microrobots were controllably and repeatedly placed in contact with the fatty acid film. This process covered the top pores of the microrobot with a thin layer of fatty acid solution, thereby sealing the loaded cargo inside the microrobot's internal chamber. Upon exposure to body temperature (37 °C), the fatty acid sealing layer would undergo a phase change from a solid to a liquid, gradually releasing the internal cargo in a prolonged and controllable manner.[33]

2.2. Tunability of Thermosensitive Fatty Acid Sealing Layer

Controlled drug release, particularly for prolonged treatment, is a clinically important goal for cardiovascular diseases. For example, in the case of arrhythmia, many patients remain on antiarrhythmic drug treatment for several years, even though many of these drugs have severe adverse effects and low efficacy.[34] Arrhythmia treatment can also consist of continuous intravenous drip, with a high degree of control over drug concentration and effect required.[35] Therefore, a highly tunable mechanism to control and prolong drug release would be useful for treating cardiovascular diseases. Phase change materials are suitable for such a mechanism because they retain a solid structure until a specific eutectic point is reached, after which they transition into the liquid phase.[32] This transition would allow for a gradual drug release profile in accordance with the melting time of the material. Fatty acids are known to be nontoxic, have high heat capacity, be noncorrosive, retain thermal/chemical stability, and have little volume change during phase transformation.[33] By utilizing the previously reported dip sealing method,[24] the microrobots were sealed with a layer composed of several fatty acids; this highly biocompatible material can slowly degrade and melt upon exposure to body temperature (37 °C), while remaining solid at room temperature (25 °C). Two different fatty acid mixtures were studied: 1) 80 wt% Lauric Acid/20 wt% Stearic Acid (abbreviated as 80%LA:20%SA) and 2) 70 wt% Lauric Acid/30 wt% Myristic Acid (abbreviated as 70%LA:30%MA). These mixtures were chosen due to their slightly different melting ranges, which allowed for the demonstration of tunable drug release based on the thermosensitivity of the sealing layer (Movie S1, S2, Supporting Information).

To generate a fatty acid sealing layer on the microrobot, we first developed a thin layer of liquid fatty acid mixture suitable for dip sealing. In brief, a thin layer of 4% w/v polystyrene dissolved in γ-Butyrolactone was spin-coated onto a glass coverslip[36] and

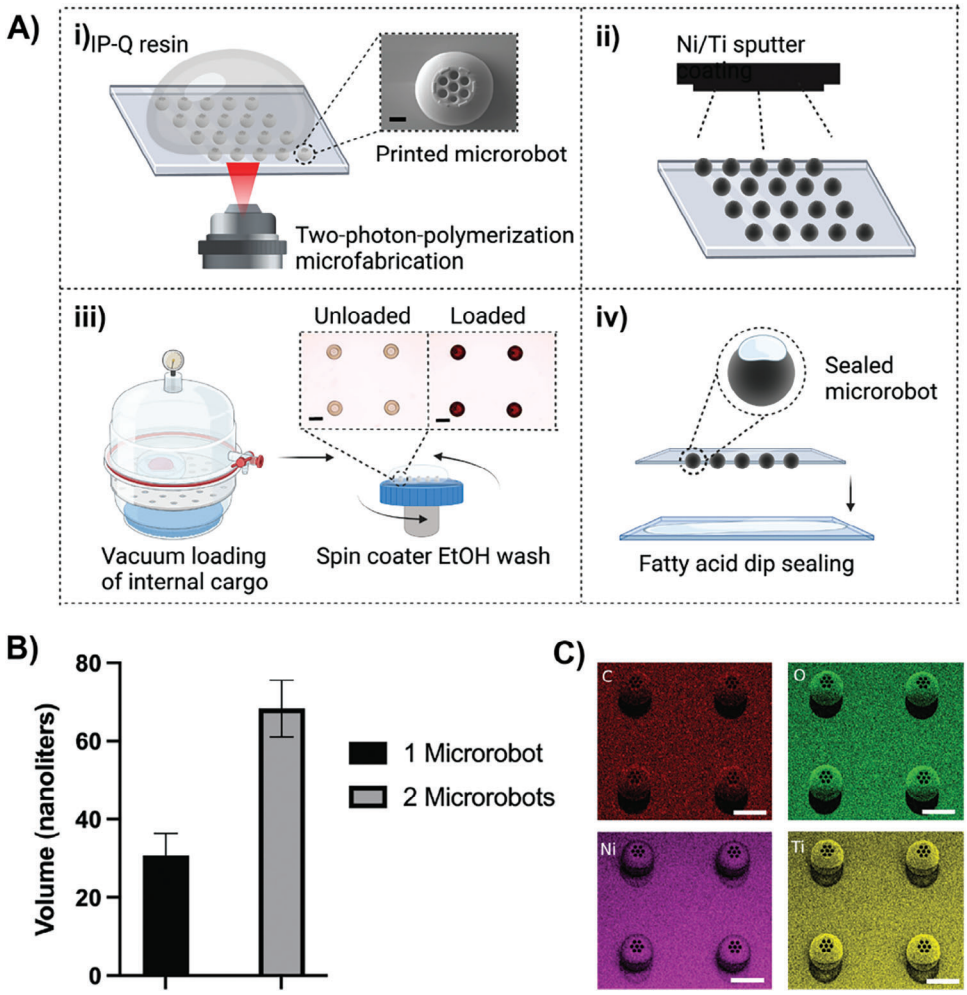

Figure 2. A) i-iv: Microfabrication, coating, vacuum loading, and dip sealing of microrobots. Scale bar = 100 μm in A(i), 500 μm in A(iii). B) Loading capacity of filled microrobots (N = 4, mean ± S.D.). C) Energy-dispersive X-ray spectroscopy shows chemical composition following magnetic deposition on the microrobot. Scale bar = 500 μm.

then used as a base upon which the liquid-state fatty acid mixture could form a uniform film via spin coating. The fatty acid film was then repeatedly mechanically transferred to the microrobots with limited force via a computer-controlled micro-manipulation machine (**Figure** 3A). After each successive contact, the microrobots were separated from the sealing substrate and allowed to cool, which caused the sealing layer on the microrobot to solidify. After four cycles of this contact, the microrobots were sufficiently sealed with a layer of the fatty acid solution. Formation of the sealing layer was confirmed under SEM microscopy, which showed complete coverage of the microrobot pores for both fatty acid mixtures immediately after dip sealing (Figure 3B). The melting range of 80%LA:20%SA and 70%LA:30%MA were measured as 36–45 and 34–41 °C, respectively (Figure 3C). Both fatty acid mixtures were solid at room temperature (Figure 3D) but demonstrated different melting performances after the sealed microrobots were incubated for 1 h in 37 °C water (Figure 3B). As expected by its lower melting range, the 70%LA:30%MA fatty acid mixture displayed a strong degree of melting with almost all microrobot pores exposed, while the 80%LA:20%SA mixture maintained some pore protection after the incubation period.

To quantify the release mechanics of the microrobots sealed with each fatty acid mixture in comparison to an unsealed microrobot, 1% w/v RhB in DMSO solution was loaded into the microrobots and used as a fluorescent reporter (Figure 3E). Unsealed microrobots demonstrated almost instantaneous cargo release, with 85.53 ± 4.72% of total cargo released within 10 min in a 37 °C aqueous environment. In comparison, microrobots sealed with the lower melting range fatty acid mixture (70%LA:30%MA) released 38.93 ± 9.76% of total cargo in 10 min while microrobots sealed with 80%LA:20%SA released 19.48 ± 4.88% of the total cargo in the same amount of time. Both sets of sealed microrobots displayed prolonged cargo release over a 2 h time period: 81.88 ± 1.16% of total cargo was released by the 70%LA:30%MA sealed microrobots and 70.70 ± 2.83% of total cargo was released by the 80%LA:20%SA sealed microrobots. Protection of internal drug cargo and prolonged release upon sealing was verified through optical imaging of the microrobots in water, where unsealed microrobots were observed to fully release cargo after 10 min as indicated by the transparency of the microrobot (Figure 3F). In comparison, both the 70%LA:30%MA and 80%LA:20%SA sealed microrobots demonstrated strong cargo

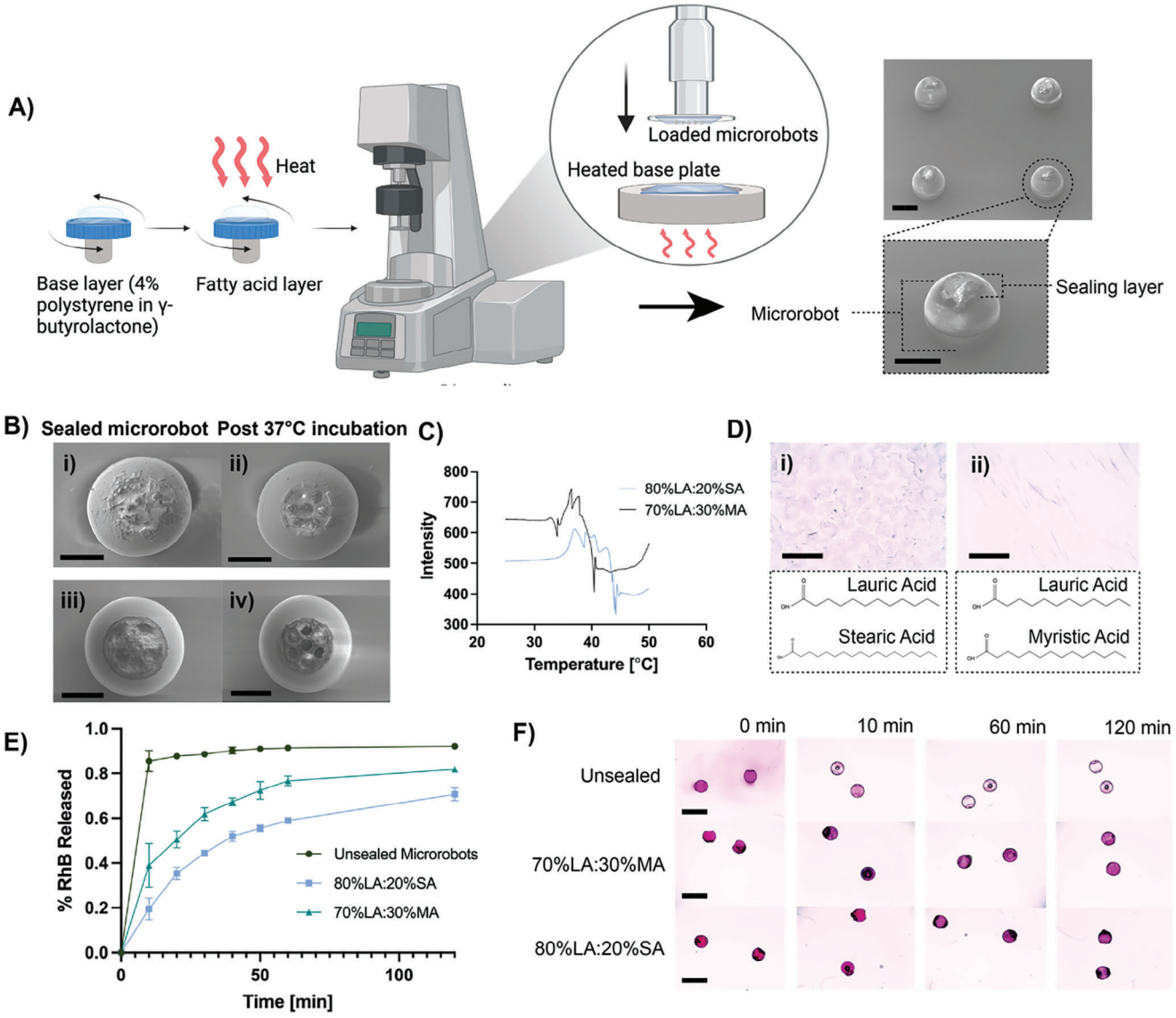

Figure 3. A) Fatty-acid sealing layer was spin-coated onto a base layer of polystyrene in γ-Butyrolactone. Microrobots were dip-sealed in an automated process. Scale bar = 200 µm) B) SEM imaging of microrobots sealed with 80%LA:20%SA before (i) and after (ii) incubation in water at 37 °C. SEM imaging of microrobots sealed with 70%LA:30%MA before (iii) and after (iv) incubation in water at 37 °C. (Scale bar = 400 µm). C) Melt curves of fatty acid sealing solutions. D) i) Brightfield imaging of 80%LA:20%SA. ii) Brightfield imaging of 70%LA:30%MA. (Scale bar = 1100 µm). E) Release curves (% RhB solution from total) of unsealed microrobots, microrobots sealed with 80%LA:20%SA, and microrobots sealed with 70%LA:30%MA (N = 4, mean ± S.D.). F) Brightfield imaging of microrobots in water at 37 °C over time. (Scale bar = 1100 µm).

protection, with visible melting of the 70%LA:30%MA after 2 h of incubation at 37 °C and subsequent faster cargo release. Altogether, these results demonstrate the thermal responsiveness and tunability of a fatty acid sealing layer to easily customize drug release. The 80%LA:20%SA sealing layer was exclusively used in subsequent experiments due to its more prolonged drug delivery profile.

2.3. Thermally Triggered Drug Release from Filled Microrobots Modulates Beating Frequency in Cardiomyocytes

To demonstrate the utility of the fillable microrobot system for cardiac drug delivery, genetically encoded calcium channel reporter (GCaMP) iPSC-CMs were used to model a cardiac tissue monolayer. GCaMP iPSC-CMs have been used to model disease, screen drugs for cardiotoxicity, discover drugs, and study cardiac development.[37] Our cardiomyocyte differentiation achieved 99% CM purity, as assessed via immunostaining for cardiac troponin (cTnT) and flow cytometry, in comparison to an iPSC-only control (Figure S2, Supporting Information). iPSC-CMs are a reproducible, physiologically similar, and efficient in vitro model of human cardiomyocytes.[38] Specifically, iPSC-CMs accurately mimic the responses of human cardiomyocytes to small molecule cardiac drugs, such as norepinephrine and isoprenaline.[39]

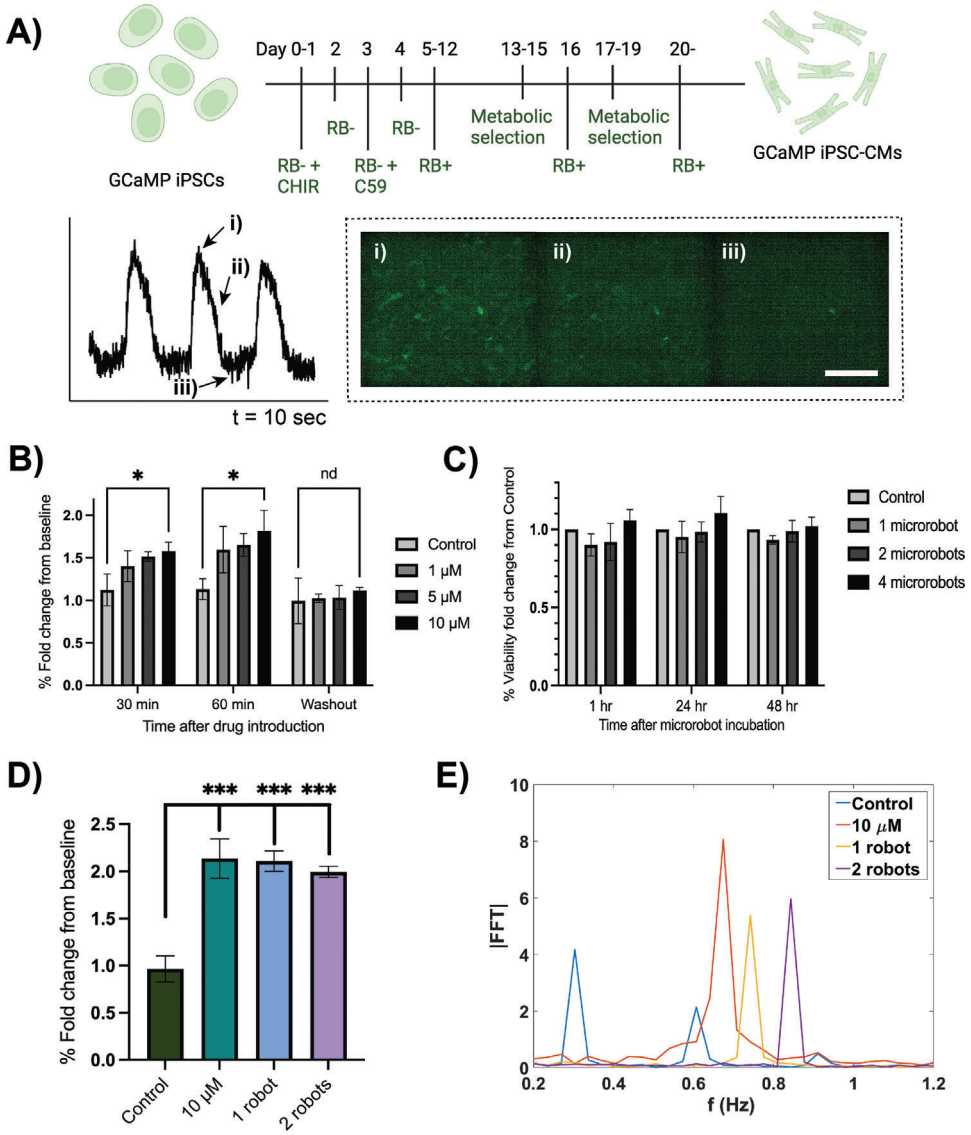

Figure 4. A) Schematic of GCaMP iPSC-CM differentiation process. Fluorescent imaging of GCaMP iPSC-CMs during i) systole, ii) midway, and iii) diastole, with corresponding beating pattern. Scale bar = 400 μm. B) Dose-dependent modulation of GCaMP iPSC-CM beating frequency with norepinephrine (N = 3, mean ± S.D., multiple unpaired *t*-test with two-stage step-up (Benjamini, Krieger, and Yekutieli) * $p < 0.05$). C) GCaMP iPSC-CM viability after microrobot introduction (N = 3, mean ± S.D.). D) Quantification of beating frequency fold change after microrobot delivery of norepinephrine in comparison to positive control (10 μM in media) (N = 4, mean ± S.D, Welch's *t*-test, *** $p < 0.05$). E) Fourier transform of GCaMP iPSC-CMs exposed to 10 μM norepinephrine in media versus drug delivery via 1 microrobot and 2 microrobots.

GCaMP is a genetically encoded fluorophore sensor of calcium, which enables imaging of cardiomyocyte beating patterns via fluorescence microscopy.[40] Because cardiomyocytes display cytosolic calcium transients in each depolarization and contractile cycle, the GCaMP reporter facilitates clear visualization of each cycle via fluorescence intensity.[41] Once differentiated, the GCaMP iPSC-CMs demonstrated high fluorescence intensity during systole, with a gradual decrease and eventual signal dissipation during diastole (**Figure** 4A). This pattern allowed for the correlation of contraction via the observed cyclic fluorescence fluctuation to quantify cardiomyocyte beating frequency.

To test the efficacy of microrobot drug delivery to the GCaMP iPSC-CMs, we selected the small molecule drug norepinephrine. Norepinephrine is known to increase cardiac output and mean arterial output in a dose-dependent manner.[42] Therefore, norepinephrine is often administered intravenously to increase blood pressure in patients with severe hypotension (low blood pressure).[43] Importantly, early administration of norepinephrine has been shown to be beneficial during septic shock, where patients can display poor cardiac contractility.[44] Delivery of norepinephrine via the microrobot system could minimize the quantity of drug needed to restore normal blood pressure for patients with hypotension or cardiogenic shock.

To quantify the effect of norepinephrine induction on GCaMP iPSC-CMs, cells were treated with a range of norepinephrine concentrations (1, 5, and 10 μM) and imaged under fluorescence

microscopy. Beating frequency was determined using a custom peak detection algorithm that quantified systolic peaks in a given period. GCaMP iPSC-CMs responded to norepinephrine simulation in a dose-dependent manner that mimicked the effect of norepinephrine on endogenous CMs. Specifically, GCaMP iPSC-CMs showed a statistically significant increase in beating frequency (relative to baseline) that persisted until washout, when frequency returned to baseline (Figure 4B).

Next, the biocompatibility of the magnetic microrobot was assessed through a resazurin-based cell viability assay (Figure 4C). The metabolic activity of GCaMP iPSC-CMs was assessed following incubation of 1, 2, or 4 microrobots inside a culture well containing cells for 1, 24, or 48 h and compared with a control group. There was no significant decrease in metabolic activity across all microrobot groups compared to the control, indicating that the introduction of microrobots to live cardiomyocytes had no deleterious effect on cell survival. This observation supported the overall biocompatibility of the microrobot platform and its future use in biological applications in the human body.

To assess the norepinephrine delivery efficacy from the loaded microrobots, 1 or 2 microrobots were introduced to GCaMP iPSC-CMs at 37 °C. As determined from the dosage titration (Figure 4B), 10 µM of norepinephrine in cell culture media was used as a positive control. The microrobot was loaded with the total amount of norepinephrine needed to achieve a final concentration of 10 µM in culture media, rendering the final drug concentration upon full cargo release to be comparable with that of the positive control. Fold change of beating frequency from baseline (per condition) was calculated, with the control demonstrating little change in frequency following the 2 h incubation period. In comparison, norepinephrine release from both microrobot conditions and the 10 µM positive control increased beating frequency by approximately twofold compared to baseline (Figure 4D). We anticipate that the leveling off of the beating frequency increase was due to the electrophysiological limitations of the GCaMP iPSC-CMs, which were observed to be unable to beat faster than ≈0.8 Hz (the calculated beating frequency following incubation with 1 robot). Moreover, the increase in beating upon norepinephrine release from the microrobots was visually confirmed through the Fourier transform of representative cardiomyocyte rhythms (Figure 4E), which also demonstrated a clear increase in beating frequency after drug introduction (Movie S3–S6, Supporting Information). These results verified that the microrobots could be successfully loaded with drug cargo (norepinephrine) and that the sealing layer on the microrobots could degrade upon prolonged exposure to a 37 °C environment, thus allowing for controlled norepinephrine release and subsequent modulation of cell beating frequency.

2.4. Microrobot Locomotion and Drug Delivery to GCaMP iPSC-CMs

Using low-intensity and high-penetration magnetic fields for magnetic actuation is a promising strategy for mobilizing microrobots to specific locations in the body, particularly in cases where there is a need to limit off-target drug effects. To achieve this, two metal layers were sequentially coated onto the microrobot surface: Ni to facilitate magnetic responsiveness, and Ti to improve biocompatibility. Due to the round shape of the microrobot, movement was accomplished through rolling or wobbling as confirmed through videography of the moving microrobot (Movie S7, S8, Supporting Information); both motions are effective in a blood-vessel-skin environment with a pipe-like cylindrical structure.[45]

To demonstrate microrobot mobility and successful drug delivery in a complex structure, two mazes were designed and fabricated using polydimethylsiloxane (PDMS) with regions seeded with GCaMP iPSC-CMs (**Figure** 5A). These cell seeding regions were interlinked via several channels (1.8 mm in diameter) mimicking native arterial dimensions and confirmed to contain cardiomyocytes by staining against cardiac troponin (Figure 5B). Each seeded region contained a highly pure population of GCaMP iPSC-CMs, which displayed phenotypical characteristics of cardiomyocytes (troponin filaments interspersed with cell nuclei) (Figure 5Biii/vi/ix/xii). These seeded regions were marked as targets for drug delivery from the microrobots. PDMS columns between the cell seeding regions and the channels constrained cardiomyocytes to the appropriate regions and limited cell adherence in the channels (Figure 5B).

Using a low intensity rotating magnetic field (10 mT), the microrobots were actuated with motion along the channel walls. Microrobots were introduced into the maze at position i) in both mazes (named T for the T-shaped maze, and L for the L-shaped maze) (Figure 5C) and guided throughout the entire maze (Figure 5D, and Movie S3, Supporting Information). As seen in the T-shaped maze, the microrobots could navigate a branching structure, demonstrating a high level of fine motor control. This ability may be particularly useful in a cardiac environment, which contains a complex vasculature that must be specifically navigated to avoid blockage. To model the effects of drug release from the microrobots within the maze, a single microrobot was maneuvered into regions T2 and L2 of each maze in a matter of seconds and remained in the specified region for the entire 2 h incubation period. At 15 min after microrobot introduction, an approximate twofold increase in beating frequency was observed, with a slightly increased frequency in regions T2 and L2 in comparison to T1 and L1 (Figure 5E). This observation was most likely due to the drug initially concentrating around the microrobot and then equilibrating after 2 h, when all four regions displayed a similar fold change in beating frequency. We anticipate that, due to diffusion in the limited maze space, norepinephrine could travel quickly from one region to another via cell culture media in the channels. Norepinephrine release from one microrobot was sufficient to cause an approximate twofold increase in beating frequency as compared to baseline in both regions (Figure 5F). While future applications may require larger drug quantities, possibly through microrobot swarms, this work demonstrates the capabilities of a single microrobot to regulate beating frequency and highlights its potential in clinical applications of arrhythmia or hypotension.

3. Conclusion

To address the unmet clinical needs of DDSs for cardiac diseases, we developed a fillable magnetic microrobot with high cargo protection and tunable, thermosensitive drug release. This biocompatible system included an internal chamber for drug

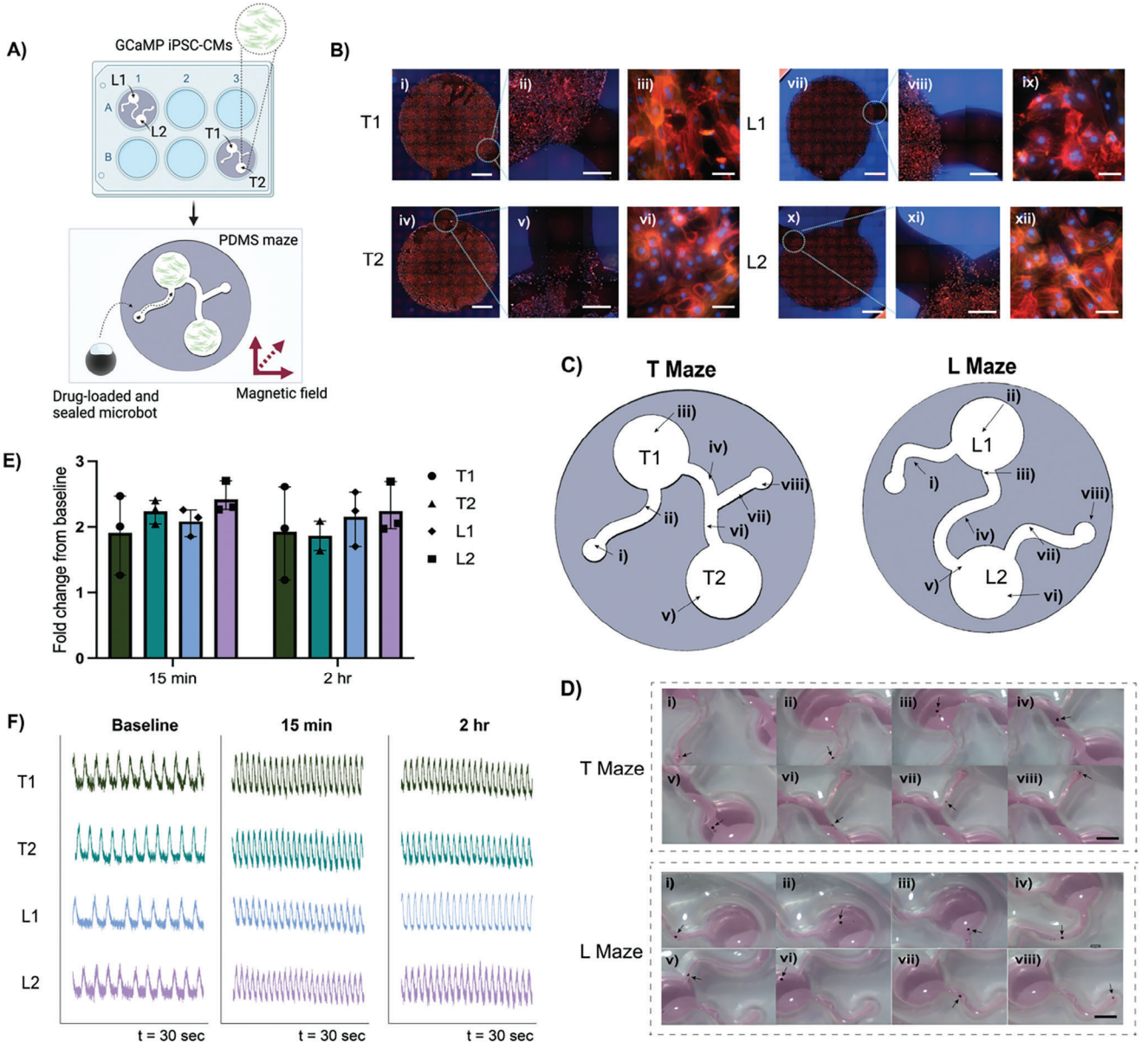

Figure 5. A) GCaMP iPSC-CMs were seeded into PDMS mazes. Microrobots were introduced into the start wells and moved via low-intensity magnetic field. B) Fluorescent imaging of GCaMP iPSC-CMs in maze well. Full well imaging (i, iv, vii, x, scale bar = 2 mm); 10× view of edge (ii, v, viii, xi, scale bar = 200 µm); 40× view of cells (iii, vi, ix, xii, scale bar = 60 µm). (Red = cardiac troponin, Orange = phalloidin, Blue = Hoescht). C) Schematic of mazes with microrobot locations throughout time. D) Magnetically guided navigation of drug-loaded and sealed microrobots through both mazes. (Scale bar = 3.6 mm) E) Quantification of fold change in beating frequency per cell seeding area in each maze after drug delivery by microrobots (individual values with mean and range, N = 2–3). F) Representative beating tracings of each well at baseline 15 min and 2 h after microrobot drug delivery.

loading, magnetic coating with Ni/Ti, and an external fatty acid sealing layer that gradually degrades upon exposure to 37 °C. 2PP-based 3D microprinting enabled uniform manufacturing of microrobot arrays, which could be loaded with drug cargo through vacuum desiccation. Using RhB as model cargo, release processes were shown to be dependent on the fatty acid composition and subsequent melting range, both of which can be tuned to achieve a faster or more prolonged release curve as desired. The microrobots were shown to be highly biocompatible with the in vitro cardiac model GCaMP iPSC-CMs and successfully modulated the beating frequency of the cardiomyocytes via norepinephrine delivery. Finally, the microrobots could be precisely steered through vascular-like maze structures containing GCaMP iPSC-CMs by using a low-intensity rotating magnetic field, suggesting that microrobots might one day be potentially mobilized through an uneven and mechanically beating surface like the heart. Based on the existing data, this microrobot system shows promise as a precise and steerable strategy for local drug delivery. Future studies in vivo are necessary to validate the activity of the magnetic microrobot in biological vessels, as well as to optimize the drug loading capabilities of the microrobot for different cardiac applications. Furthermore, the microrobots can

potentially be coupled with existing catheterization technologies to more easily enable microrobot delivery to the site of interest, with magnetically controlled motion within that specific site. All in all, our microrobot platform represents a highly customizable system with the ability to satisfy several unmet challenges in cardiac drug delivery.

4. Experimental Section

Materials: All chemical reagents were used without modification or purification unless mentioned. IP-Q resin (Nanoscribe) was used to fabricate the microrobot body. To clean the substrate, water (Millipore Milli-Q Integral 3) and acetone (VWR 20066.330) were used, with Propylene glycol methyl ether acetate (PGMEA, Sigma-Aldrich 484431) and isopropanol (IPA, Fisher Chemical P/7500/17) used to clean off any remaining resin. 1% w/v Rhodamine B (RhB; Sigma-Aldrich R6626) in dimethyl sulfoxide (DMSO, VWR 23500.260) was used as a mock loading cargo. 3-(trimethoxysilyl)propyl methacrylate (Sigma-Aldrich 440159) and ethanol (EtOH; VWR 20821.330) were used for the surface treatment of ITO glass. EtOH was used to clean the residual loading solution from the filled microrobots. As a base layer for the fatty acid sealing solution, 4% w/v polystyrene (Fisher Scientific) dissolved in γ-Butyrolactone (Sigma Aldrich B103608) was used. The fatty acids lauric acid (Sigma Aldrich W261408), stearic acid (Sigma Aldrich 175366), and myristic acid (Sigma Aldrich M3128) were used to seal the microrobots. GCaMP iPSCs (WTC-GCaMP6f) were obtained from Bruce Conklin at the J. David Gladstone Institute and differentiated to cardiomyocytes using the following reagents: Essential 8 Media (Thermofisher A1517001), CHIR (Tebu-Bio, 04-0004-02), RPMI 1640 media (Thermofisher 11875093) supplemented with B27 without insulin (Thermofisher A1895601), C59 (Stratech, S7037-SEL), and RPMI 1640 media (Thermofisher 11875093) supplemented with B27 (Thermofisher 17504044) were used to complete differentiation into cardiomyocytes. PrestoBlue reagent (Thermofisher A13261) was used to quantify cell viability. The antibodies mouse anti-cardiac troponin (BD Pharmigen 565744), isotype control (BD Pharmigen 557732), and Hoescht (Thermofisher 62249) were used for immunofluorescence microscopy and/or flow cytometry. Norepinephrine hydrochloride (Sigma Aldrich A7256) was dissolved in DMSO and used as drug cargo.

Microrobot Fabrication: To generate the microrobots, the 2PP-based 3D microprinting technique was chosen to provide high resolution in microscale. A commercial 2PP printer (Photonic Professional GT2, Nanoscribe) was used to print the microrobotic structure using the commercial resin IP-Q. The microrobot model was designed in a commercial computer-aided design software (Autodesk Inventor 2023), and further processed in a job preparation program (Describe 2.7, Nanoscribe). An ITO-coated glass was activated by O_2 plasma for 5 min and further immersed into a solution of ethanol and 3-(trimethoxysilyl)propyl methacrylate (at a ratio of 1/5 v/v) for 2 h to improve the adhesion for printed structures. The treated glass was then used as the substrate for the printing using a 10× NA 0.3 objective. After printing, the entire substrate was submerged in PGMEA for 1 h, and subsequently in IPA for 10 min. Once fully cleaned and dried, the printed microrobot array was post-cured under UV light (Form Cure λ = 405 nm) for 2 h. For magnetic control, 800 nm Ni was first deposited onto the microrobot surface, followed by deposition of 50 nm thickness Ti by sputter coating (HEX Korvus Technology).

Drug Loading and Optical Imaging: Printed microrobots were loaded into a vacuum desiccator with 100 µL of 1% w/v RhB in DMSO or norepinephrine in DMSO. Vacuum pressure facilitated solution entry via the pore array on the top of the microrobot. The loading solution was pulled down for 7 min, after which the excess RhB solution was removed and the microrobots washed using 200 µL of EtOH on a spin coater (Laurell Technologies) for 15 s at 1000 rpm. Loaded microrobots were stored at −20 °C to prevent evaporation of the loaded cargo. To measure the total cargo volume per microrobot, unsealed microrobots were allowed to release their cargo in water. The fluorescent signal (excitation wavelength at 546 nm, emission wavelength at 568 nm) was quantified and matched to a standard curve of RhB in water to determine loading volume. Microrobots were imaged under a light microscope (Evos XL Core) at 10× magnification.

Microrobot Dip Sealing: Two sealing solutions comprised of fatty acids were prepared by weight: 70 wt% Lauric Acid/30 wt% Myristic Acid, 80 wt% Lauric Acid/20 wt% Stearic Acid. Solutions were melted at 60 °C into liquid form. Glass microscope slides (Marienfeld 1100420) were spread with 4% w/v polystyrene in γ-Butyrolactone through spin coating for 30 s at 1000 rpm (RT) with 500 rpm ramp, then allowed to dry for 9 min at 90 °C. The fatty acid mixture of choice was coated onto the polystyrene layer by spin coating for 15 s at 700 rpm (50 °C) with 500 rpm ramp, then immediately used for dip sealing. A rheometer (Anton Paar Modular Compact Rheometer, MCR 302) was used to mechanically dip seal the microrobot with the fatty acid mixture. The microrobots were attached to the top parallel plate, while the sealing layer was placed on the bottom plate (heated at 50 °C to maintain fluidity). The microrobots were mechanically lowered to make contact with the base, after which the top plate would move upward, causing a layer of the sealing mixture to adhere to the microrobot surface. This process minimized contact force to prevent microrobot fracturing and was repeated four times for successful sealing.

Melting Range Analysis: The melting range of the two fatty acid sealing solutions was assessed using a digital melting point apparatus (Cole-Palmer ML-03013-02 SMP50) by loading the sealing solution in liquid form via a syringe into glass capillaries. The temperature range was set at 25 to 50 °C, with a 5 °C per minute temperature ramp up. Melt curves were analyzed and melting range was calculated.

Drug Release: Four sealed microrobots were carefully removed via pipette from the substrate slide and immersed in 267 µL of pure water. The solution was placed in a shaker (Eppendorf Thermomixer C) at 37 °C with a 300 rpm shaking speed. At each time point, 200 µL of the water was removed for analysis by Spectramax M5 plate reader (Molecular Devices) with an excitation wavelength of 546 nm and an emission wavelength of 568 nm, after which all the water in the tube was replaced with fresh solution for the next time point. Microrobots were imaged with a light inverted microscope (Evos XL Core) using a 10× objective at each release time point.

Microrobot Imaging and Mapping: The microrobots were completely dried, sputter coated with Cr (40 nm), and imaged through scanning electron microscopy (JEOL 6010LA, LG05E2). To determine the elemental composition (C, O, Ni, Ti) on the microrobot, energy-dispersive X ray spectroscopy (EDX mapping) was conducted.

GCaMP iPSC-CM Differentiation and Cell Culture: GCaMP iPSCs were cultured in Essential 8 media in Matrigel (Corning 1:160, diluted in RPMI 1640 basal media) coated plates until ≈80% confluency. After splitting, cells were switched to RPMI 1640 media supplemented with B27 without insulin (RB-) with 0.6 µL mL^{-1} CHIR. 1 day later (Day 1), media was switched to RB-. On Day 2, media was switched to RB- with 0.25 µL mL^{-1} C59. On Day 3, media was switched to RB- media. On Day 4, media was switched to RPMI media supplemented with B27 with insulin (Thermofisher) (RB+). Cells were cultured until beating (around Day 7), after which two rounds of metabolic selection was conducted using RPMI media without glucose (Thermofisher 11879020) supplemented with B27 with insulin. GCaMP iPSC-CMs were maintained in RB+ media until replated or used for experiments.

Flow Cytometry: GCaMP iPSC-CMs were detached with 0.7 mg mL^{-1} Type II collagenase (ThermoFisher Scientific, 17101015) and GCaMP iPSCs were detached with 5 mM EDTA (Life Technology, 15575-020); both were washed twice with phosphate buffered saline (PBS). Cells were fixed with 4% v/v paraformaldehyde (PFA, ThermoFisher Scientific, 28908) for 10 min, then permeabilized with 0.1% v/v Triton-X (Sigma-Aldrich, X100) for 10 min. To analyze cardiomyocyte purity, cardiac troponin antibody (BD Bioscience, 565744) and an isotype control (BD Bioscience, 557732) were diluted 1:400 in 2% v/v fetal bovine serum (FBS) in PBS and incubated with cells overnight; cells were then washed twice with 2% v/v FBS in PBS and analyzed via flow cytometry (LSR Fortessa 1, Becton Dickinson).

Norepinephrine Titration: GCaMP iPSC-CMs were replated in a Matrigel-coated 24 well plate at a density of 300 000 cells well^{-1}. After cells commenced beating, cells were washed and media was changed to norepinephrine dissolved in sterile DMSO diluted to several concentrations (1, 5, 10 µM) in RB+ media. Cells were incubated at 37 °C in this solution and imaged at baseline (pre-drug introduction), 30 min, and 60 min after drug introduction on a live-cell imaging microscope (Zeiss Axio Imager 2). 30 second recordings of cell beating were taken of each well at each timepoint. After 60 min, cells were washed 2× with PBS and a washout recording was taken 2 h afterward. Beating frequencies were determined by selecting cell regions of interest in FIJI (3 regions with cell beating, 3 regions as background) and using the multi-measure function to determine intensities per millisecond. Using a custom MATLAB script, these intensities were plotted to determine how many peaks occurred per 30 s recording, which determined beating frequency in Hz. Fold change from baseline was used to quantify any drug effects on beating frequency.

Cell Viability: Sputter-coated microrobots were loaded with 313 mM norepinephrine in DMSO and sealed with 80% Lauric acid/20% Stearic acid. Sealed microrobots were sterilized under UV light for 30 min. One, two, or four microrobots were added per well in a 24 well plate seeded with GCaMP iPSC-CMs (300 000 cells well^{-1}) for three microrobot conditions in comparison to an untreated set of wells. After 1 h of incubation at 37 °C, microrobots were removed, cells were washed with PBS, and RB+ media was replaced. Cell viability was assessed through PrestoBlue at 1, 24, and 48 h after incubation. Fluorescent readings were taken at an excitation of 560 nm and emission of 590 nm on a plate reader (Spectramax M5, Molecular Devices), then fold change from control was calculated.

Microrobot Drug Release in GCaMP iPSC-CMs: Two sealed and sterilized microrobots were added to one well of a 24 well plate seeded (300 000 cells well^{-1}) with GCaMP iPSC-CMs for an approximate final drug concentration of 10 µM. Beating frequency was assessed via live-cell imaging at baseline (before drug/microrobot introduction) and after 2 h of incubation. 10 µM of norepinephrine diluted in RB+ was used as a positive control, with untreated wells as a negative control. Beating frequencies were quantified as previously described.

Maze Casting, Seeding, and Imaging: Maze designs were generated on Solidworks and printed with resin on a Prusa SL1S 3D printer (Prusa 3D). Negative casts were generated using Ecoflex (Smooth On, 00–30) and treated with Trichloro(1H,1H,2H,2H-perfluorooctyl)silane. Final molds were cast with poly(dimethylsiloxane) (PDMS). The PDMS molds were adhered to 6 well cell culture plates by spreading a thin layer of PDMS on the bottom of the mold and curing the mold to the plate by baking at 65 °C overnight. Mold-bonded plates were sterilized under UV light for 1 h and coated with Matrigel. GCaMP iPSC-CMs were seeded at a density of 250 000 cells cm^{-2}. To image the mazes, cells were fixed with 4% v/v PFA overnight at 4 °C. Wells with cells were permeabilized/blocked with 5% v/v bovine serum albumin and 0.3% v/v Triton-X in PBS for 15 min at room temperature. Cells were stained with Hoescht (1:250) and cardiac troponin (1:400) in perm/block solution overnight on a rocker at 4 °C. After washing (two times with 0.1% v/v Triton-X in PBS for 15 min each, then one time with PBS for 15 min), cells were imaged on the Leica live-cell imaging microscope.

Microrobot Mobility: To demonstrate microrobot mobility under a magnetic field, seeded mazes with microrobots in the starting maze wells were placed over a Minimag Rev. A (Pantec) that could generate three degrees of positional freedom and variable magnetic fields (0-20 mT). The magnetic field (MFG-100-I, Magnebotix) was controlled by varying the inclination and azimuth rotational axes. Field intensity was kept constant at 10 mT for all experiments, and motion was recorded through a puA2500-14uc charge-coupled device camera (Basler Pulse).

Statistical Analyses: All statistical analyses were conducted in Graphpad. All comparisons were done using unpaired two-tailed Student's T test with Welch correction, one-way ANOVA, or multiple unpaired *t*-tests with false discovery rate and two-stage step-up (Benjamin, Krieger, and Yekutieli). $p<0.05$ was considered statistically significant. "ns" represents non-significant, * $p < 0.05$, *** $p < 0.005$.

Schematics: All schematics were generated in Biorender.

Supporting Information

Supporting Information is available from the Wiley Online Library or from the author.

Acknowledgements

M.S.C. acknowledges funding from the British Marshall Scholarship. R.W. and M.M.S. acknowledge funding from The Rosetrees Trust under the Young Enterprise Fellowship agreement (A2741/M873) and the British Heart Foundation under the Centre of Research Excellence agreement (RE/18/4/34215). J.K. acknowledges the support of the Korea Health Industry Development Institute (KHIDI) grant (HI19C1095) and National Research Foundation (NRF) grant (2022R1A6A3A03069072) funded by the Korean Government. M.M.S. acknowledges support from the Department of Science, Innovation and Technology (DSIT) and the Royal Academy of Engineering under the Chair in Emerging Technologies programme (CiET2021\94). The authors acknowledge access to SEM facilities at the Harvey Flower Electron Microscopy Suite (Department of Materials, Imperial College London). For the purpose of open access, the authors have applied a Creative Commons Attribution (CC BY) license to any Author Accepted Manuscript version arising.

Conflict of Interest

The authors declare no conflict of interest.

Author Contributions

M.S.C. and R.S. contributed equally to this work. M.S.C., R.S., R.W., and M.M.S. conceived and designed this work. M.S.C. performed the experiments with guidance from R.S. and R.W. K.Z., Y.Z., J.K. assisted with data collection and provided conceptual advice. All authors discussed results and assisted in the preparation of the paper. M.S.C. drafted the manuscript; R.S., R.W. K.Z., Y.Z., J.K., and M.M.S. revised the paper. M.M.S. supervised the study. All authors have given approval to the final version of the manuscript.

Data Availability Statement

The data that support the findings of this study are available from the corresponding author upon reasonable request.

Keywords

cardiac arrhythmias, fillable microrobots, magnetic actuation, phase-change materials, stimuli-responsive drug delivery

Received: February 2, 2024
Revised: May 5, 2024
Published online:

[1] Y. Han, H. Xie, Y. Liu, P. Gao, X. Yang, Z. Shen, *Cardiovasc. Diabetol.* **2019**, *18*, 96.
[2] R. C. Scott, D. Crabbe, B. Krynska, R. Ansari, M. F. Kiani, *Expert Opin Drug Deliv* **2008**, *5*, 459.
[3] B. Qian, Q. Zhao, X. Ye, *J. Cardiovasc. Pharmacol.* **2020**, *76*, 414.
[4] S. Rao, A. Tan, N. Thomas, C. A. Prestidge, *J Control Release* **2014**, *193*, 174.

[5] X. Liao, X. Yang, H. Deng, Y. Hao, L. Mao, R. Zhang, W. Liao, M. Yuan, *Front. Bioeng. Biotechnol.* **2020**, *8*, 251.
[6] L. Saludas, C. C. Oliveira, C. Roncal, A. Ruiz-Villalba, F. Prosper, E. Garbayo, M. J. Blanco-Prieto, *Nanomaterials (Basel)* **2021**, *11*, 570.
[7] D. J. Lundy, K. H. Chen, E. K. Toh, P. C. Hsieh, *Sci. Rep.* **2016**, *6*, 25613.
[8] M. Dunne, B. Epp-Ducharme, A. M. Sofias, M. Regenold, D. N. Dubins, C. Allen, *J. Control Release* **2019**, *308*, 197.
[9] L. Palanikumar, S. Al-Hosani, M. Kalmouni, V. P. Nguyen, L. Ali, R. Pasricha, F. N. Barrera, M. Magzoub, *Commun. Biol.* **2020**, *3*, 95.
[10] P. M. Perrigue, R. A. Murray, A. Mielcarek, A. Henschke, S. E. Moya, *Pharmaceutics* **2021**, *13*, 770.
[11] V. P. Torchilin, J. Narula, E. Halpern, B. A. Khaw, *Biochim. Biophys. Acta* **1996**, *1279*, 75.
[12] M. Y. Chang, Y. J. Yang, C. H. Chang, A. C. Tang, W. Y. Liao, F. Y. Cheng, C. S. Yeh, J. J. Lai, P. S. Stayton, P. C. Hsieh, *J. Control Release* **2013**, *170*, 287.
[13] H. Su, S. Li, G.-Z. Yang, K. Qian, *Adv. Healthcare Mater.* **2023**, *12*, 2202391.
[14] F. Xie, R. Li, W. Shu, L. Zhao, J. Wan, *Materials Today Bio 14*, 100239.
[15] F. M. van der Valk, D. F. van Wijk, M. E. Lobatto, H. J. Verberne, G. Storm, M. C. Willems, D. A. Legemate, A. J. Nederveen, C. Calcagno, V. Mani, S. Ramachandran, M. P. Paridaans, M. J. Otten, G. M. Dallinga-Thie, Z. A. Fayad, M. Nieuwdorp, D. M. Schulte, J. M. Metselaar, W. J. Mulder, E. S. Stroes, *Nanomedicine* **2015**, *11*, 1039.
[16] N. A. Mohamed, I. Marei, S. Crovella, H. Abou-Saleh, *Int. J. Mol. Sci.* **2022**, *23*, 1404.
[17] Y. L. Liu, D. Chen, P. Shang, D. C. Yin, *J. Control Release* **2019**, *302*, 90.
[18] J. F. Liu, B. Jang, D. Issadore, A. Tsourkas, *Wiley Interdiscip. Rev. Nanomed. Nanobiotechnol.* **2019**, *11*, e1571.
[19] C. Limpabandhu, Y. Hu, H. Ren, W. Song, Z. T. Ho Tse, *Proc. Inst. Mech. Eng. H* **2023**, *237*, 297.
[20] S. Sahoo, T. Kariya, K. Ishikawa, *Nat. Rev. Cardiol.* **2021**, *18*, 389.
[21] C. C. Nguyen, M. T. Thai, T. T. Hoang, J. Davies, P. T. Phan, K. Zhu, L. Wu, M. A. Brodie, D. Tsai, Q. P. Ha, H.-P. Phan, N. H. Lovell, T. Nho Do, *Sens. Actuators, A* **2023**, *357*, 114380.
[22] R. Dreyfus, Q. Boehler, S. Lyttle, P. Gruber, J. Lussi, C. Chautems, S. Gervasoni, J. Berberat, D. Seibold, N. Ochsenbein-Kölble, M. Reinehr, M. Weisskopf, L. Remonda, B. J. Nelson, *Sci. Rob.* **2024**, *9*, eadh0298.
[23] J. Rogatinsky, D. Recco, J. Feichtmeier, Y. Kang, N. Kneier, P. Hammer, E. O'Leary, D. Mah, D. Hoganson, N. V. Vasilyev, T. Ranzani, *Sci. Adv.* **2023**, *9*, eadi5559.
[24] X. Song, R. Sun, R. Wang, K. Zhou, R. Xie, J. Lin, D. Georgiev, A.-A. Paraschiv, R. Zhao, M. M. Stevens, *Adv. Mater.* **2022**, *34*, 2204791.
[25] M. Muneeb, N. Nuzhat, A. Khan Niazi, A. H. Khan, Z. Chatha, T. Kazmi, S. Farhat, *Cureus* **2023**, *15*, e46606.
[26] A.-I. Bunea, N. del Castillo Iniesta, A. Droumpali, A. E. Wetzel, E. Engay, R. Taboryski, *Micro* **2021**, *1*, 164.
[27] A. O. Fung, V. Kapadia, E. Pierstorff, D. Ho, Y. Chen, *J. Phys. Chem. C* **2008**, *112*, 15085.
[28] M. P. Casaletto, G. M. Ingo, S. Kaciulis, G. Mattogno, L. Pandolfi, G. Scavia, *Appl. Surf. Sci.* **2001**, *172*, 167.
[29] J. Markhoff, M. Krogull, C. Schulze, C. Rotsch, S. Hunger, R. Bader, *Materials* **2017**, *10*, 52.
[30] R. Sun, X. Song, K. Zhou, Y. Zuo, R. Wang, O. Rifaie-Graham, D. J. Peeler, R. Xie, Y. Leng, H. Geng, G. Brachi, Y. Ma, Y. Liu, L. Barron, M. M. Stevens, *Adv. Mater.* **2023**, *35*, 2207791.
[31] H. Zhu, P. Zhang, Z. Meng, M. Li, *J. Nanosci. Nanotechnol.* **2015**, *15*, 3288.
[32] D. Rozanna, T. G. Chuah, A. Salmiah, T. S. Y. Choong, M. Sa'ari, *Int. J. Green Energy* **2005**, *1*, 495.
[33] Z. Fan, Y. Zhao, X. Liu, Y. Shi, D. Jiang, *ACS Omega* **2022**, *7*, 16097.
[34] J. Larson, L. Rich, A. Deshmukh, E. C. Judge, J. J. Liang, *J. Clin. Med.* **2022**, *11*, 3233.
[35] P. Zimetbaum, *Circulation* **2012**, *125*, 381.
[36] Y. Wang, J. Balowski, C. Phillips, R. Phillips, C. E. Sims, N. L. Allbritton, *Lab Chip* **2011**, *11*, 3089.
[37] I. Karakikes, M. Ameen, V. Termglinchan, J. C. Wu, *Circ. Res.* **2015**, *117*, 80.
[38] P. Pushp, D. E. S. Nogueira, C. A. V. Rodrigues, F. C. Ferreira, J. M. S. Cabral, M. K. Gupta, *Stem Cell Rev. Rep.* **2021**, *17*, 748.
[39] a) E. G. Navarrete, P. Liang, F. Lan, V. Sanchez-Freire, C. Simmons, T. Gong, A. Sharma, P. W. Burridge, B. Patlolla, A. S. Lee, H. Wu, R. E. Beygui, S. M. Wu, R. C. Robbins, D. M. Bers, J. C. Wu, *Circulation* **2013**, *128*,. b) A. Mehta, Y. Y. Chung, A. Ng, F. Iskandar, S. Atan, H. Wei, G. Dusting, W. Sun, P. Wong, W. Shim, *Cardiovasc. Res.* **2011**, *91*, 577.
[40] a) C. N. Broyles, P. Robinson, M. J. Daniels, *Cells* **2018**, 7; b) T. W. Chen, T. J. Wardill, Y. Sun, S. R. Pulver, S. L. Renninger, A. Baohan, E. R. Schreiter, R. A. Kerr, M. B. Orger, V. Jayaraman, L. L. Looger, K. Svoboda, D. S. Kim, *Nature* **2013**, *499*, 295.
[41] W. Z. Zhu, D. Filice, N. J. Palpant, M. A. Laflamme, *Methods Mol. Biol.* **2014**, *1181*, 229.
[42] C. Martin, L. Papazian, G. Perrin, P. Saux, F. Gouin, *Chest* **1993**, *103*, 1826.
[43] D. D. Backer, P. Biston, J. Devriendt, C. Madl, D. Chochrad, C. Aldecoa, A. Brasseur, P. Defrance, P. Gottignies, J. L. Vincent, S. I. Investigators, *N. Engl. J. Med.* **2010**, *362*, 779.
[44] O. Hamzaoui, J. F. Georger, X. Monnet, H. Ksouri, J. Maizel, C. Richard, J. L. Teboul, *Crit. Care* **2010**, *14*, R142.
[45] L. Yang, T. Zhang, R. Tan, X. Yang, D. Guo, Y. Feng, H. Ren, Y. Tang, W. Shang, Y. Shen, *Adv. Sci. (Weinh)* **2022**, *9*, e2200342.